Computers & Fluids 46 (2011) 78–87

Contents lists available at ScienceDirect

Computers & Fluids

journal homepage: www.elsevier.com/locate/compfluid

Efficient shape optimization for certain and uncertain aerodynamic design

Claudia Schillings, Stephan Schmidt, Volker Schulz *

Universität Trier, Universitätsring 15, D-54296 Trier, Germany

ARTICLE INFO

Article history:
Received 4 May 2010
Received in revised form 3 December 2010
Accepted 7 December 2010
Available online 13 December 2010

Keywords:
Aerodynamic shape optimization
Shape calculus
Aleatoric uncertainties
Nonlinear stochastic programming

ABSTRACT

In this paper, we present novel developments in aerodynamic shape optimization based on shape calculus as well as the proper treatment of aleatoric uncertainties in the field of aerodynamic design.

1. Introduction

Aerodynamic shape optimization is a very active research field facing the challenges from highly demanding computational fluid dynamics (CFD) problems, from optimization with partial differential equations (PDE) as constraints, as well as from the proper treatment of uncertainties. This is particularly the case in aerodynamic aircraft design. In this contribution, we focus on novel developments in highly efficient deterministic numerical optimization methods based on shape calculus and in the efficient treatment of uncertainties in aerodynamic design based on discretized semi-infinite approaches in combination with problem dependent sparse grid techniques.

The state-of-the-art in aerodynamic design is defined by deterministic gradient based parametric design optimization, where the gradient information is produced by an adjoint approach and the arising optimization problems are solved in a one-shot approach [1]. These approaches suffer from the following deficits: When the level of detail of the geometric resolution is increased beyond some handfuls of geometric parameters, the unavoidable construction of mesh sensitivities becomes a major bottleneck and impedes the algorithmic efficiency significantly. Furthermore, a deterministic parametric approach ignores the fact that the exact conditions of operation of the optimal geometric structure are far less exactly known as one might think: the macroscopic Mach number, the angle of incident and other constants are known to lie in a certain range, rather not at a certain point, the geometry itself undergoes unknown operational changes due to wear and tear and manufacturing inaccuracies. All these deviations from assumed set-points during the deterministic optimization, may render the supposedly optimal solution worthless.

Therefore, this paper gives insight into significant enhancements of gradient based shape optimization methods aiming at removing the deficits of state-of-the-art methods outlined above. We show in Section 2, how shape calculus can be exploited in order to compute optimal geometries for aircrafts with arbitrary resolution with an algorithmic performance comparable to the conventional parametric optimization approaches. In Section 3, we attack the additional computational complexity of the treatment of uncertainties in parametric optimal design. Ideally, both enhancements to the state-of-the-art should be combined to a robust approach to shape optimization based on shape calculus. This topic is under current research and there will be further publications devoted to this issue.

2. Deterministic aerodynamic design based on shape calculus

2.1. Overview on shape sensitivity analysis

Shape calculus summarizes the mathematical framework, when the shape of an object is the unknown quantity and should be determined in accordance to a certain (differentiable) goal. For a gradient based optimization approach the sensitivity information of an objective function is needed with respect to the shape of the boundary it is defined on, which is often termed "shape sensitivity analysis". While these methods have been used quite successfully to derive theoretical results for optimal shapes, such as

* Corresponding author. Address: Universität Trier, FB IV, Abteilung Mathematik, Universitätsring 15, D-54296 Trier, Germany. Tel.: +49 651 201 3484; fax.: +49 651 201 3966.
E-mail address: volker.schulz@uni-trier.de (V. Schulz).

0045-7930/$ - see front matter © 2010 Elsevier Ltd. All rights reserved.
doi:10.1016/j.compfluid.2010.12.007

the optimal supersonic Haak body [2] or the rugby-ball ogive shapes in a Stokes flow [3], most numerical schemes are actually based on smooth ansatz functions such as the very popular Hicks–Henne functions [4] or other curve parameterizations such as b-splines.

Here, however, we use the non-parametric shape sensitivity approach to numerically conduct large scale shape optimization. In the following, let the domain under consideration be given by $\Omega \subset \mathbb{R}^3$ compact with sufficiently smooth boundary $\Gamma := \partial\Omega$. We seek to compute the derivative or sensitivity information of general objective functions such as

$$J_1(\Omega) := \int_\Omega f \, dA \tag{1}$$

$$J_2(\Omega) := \int_\Gamma g \, dS \tag{2}$$

with respect to the domain Ω, where f and g are sufficiently smooth functions. To this end, a deformed domain

$$\Omega_t = T_t(\Omega) = \{T_t(x) : x \in \Omega\}$$

is considered. The family of bijective mappings T_t is usually chosen as the perturbation of identity

$$T_t(x) = x + tV(x) \tag{3}$$

or the speed method, where T_t is the solution of the differential equation

$$\frac{\partial x}{\partial t} = V(t,x), \; x(0) = x_0 \in \Gamma. \tag{4}$$

In the shape optimization context, Eq. (4) is sometimes called "flow equation", which is not the be confused with the fluid state equation in the context of computational fluid dynamics. Furthermore, V is a sufficiently smooth vector field that takes the role of the differentiation direction. For the volume case (1), it is easy to see that

$$\begin{aligned}\int_{\Omega_t} f \, dA_t &= \int_\Omega f(T_t(x)) \sqrt{\det DT_t^T DT_t(x)} \, dA(x) \\ &= \int_\Omega f(T_t(x)) |\det DT_t(x)| \, dA(x),\end{aligned}$$

which can easily be differentiated with respect to t:

$$\begin{aligned}dJ_1(\Omega)[V] &= \int_\Omega \frac{d}{dt}\Big| f(T_t(x)) \det(DT_t(x)) \, dA(x) \\ &= \int_\Omega \langle \nabla f(x), V(x)\rangle + f(x) \mathrm{div} V(x) \, dA(x) \\ &= \int_\Omega \mathrm{div}(f(x)V(x)) \, dA(x).\end{aligned} \tag{5}$$

A similar computation for the surface objective function results in

$$\begin{aligned}dJ_2(\Omega)[V] &= \frac{d}{dt}\Big| \int_{\Gamma_t} g \, dS_t = \int_\Gamma \langle \nabla g, V\rangle + g \cdot (\mathrm{div} V - \langle DVn, n\rangle) \, dS \\ &= \int_\Gamma \langle \nabla g, V\rangle + g \mathrm{div}[\Gamma] V \, dS,\end{aligned} \tag{6}$$

where div_Γ is the tangential or surface divergence operator. Thus, the sensitivity equations (5) and (6) can be interpreted as the directional derivatives in direction V.

2.2. The Hadamard formula

The Hadamard theorem or Hadamard–Zolésio structure theorem [5,6] states that under some regularity assumptions, the sensitivity equations (5) and (6) can be expressed as a scalar product of the normal component of the perturbation field V with some shape gradient on the surface of the geometric object to be optimized, i.e.

$$dJ(\Omega)[V] = dJ(\Gamma)[\langle V, n\rangle n].$$

For the volume case (5) applying the divergence theorem results in

$$dJ_1(\Omega)[V] = \int_\Gamma \langle V, n\rangle \, f \, dS.$$

The surface case, Eq. (6), requires elements form tangential calculus, especially the tangential Stokes formula. However, one can show that

$$dJ_2(\Omega)[V] = \int_\Gamma \langle V, n\rangle \left[\frac{\partial g}{\partial n} + \kappa g\right] \, dS,$$

where $\kappa := \mathrm{div}[\Gamma] n$ is the additive mean curvature. Thus, formulas are created which can be very efficiently evaluated numerically allowing a large scale shape optimization. The need to compute mesh sensitivity Jacobians is completely circumvented. Instead, some geometric quantities such as the curvature κ must be computed, which can be conveniently done using discrete differential geometry [7].

For the application in computational fluid dynamics and aerodynamic design, the above formula become more complex, because the usual objective functions such as fluid forces in addition to a dependence on the PDE fluid state also depend on the geometry and these quantities must be differentiated accordingly. For a dependence on the normal, one has

$$J(g, \Gamma) := \int_\Gamma g(\varphi, D\varphi, n) \, dS,$$

where $g : \mathbb{R}^d \times \mathbb{R}^{d\times d} \times \mathbb{R}^d \to \mathbb{R}, (\varphi, \zeta, \psi) \mapsto g(\varphi, \zeta, \psi)$ is a sufficiently smooth functional. The shape derivative of the above expression is then given by

$$\begin{aligned}dJ(g,\Gamma)[V] = &\int_\Gamma \langle V, n\rangle [D_\varphi g D\varphi n + D_\zeta g D^2 \varphi n + \kappa(g - D_\psi g n) \\ &+ \mathrm{div}[\Gamma](D_\psi g)^T] dS.\end{aligned}$$

2.3. Shape optimization and the incompressible Navier–Stokes equations

The incompressible Navier–Stokes equations are considered in a general setting:

$$\begin{aligned}\min_{(u,p,\Omega)} J(u,p,\Omega) := &\int_\Omega f(u, Du, p) dA \\ &+ \int_{\Gamma_0} g(u, D_n u, p, n) dS \\ \text{subject to} \; -\mu\Delta u + \rho u \nabla u + \nabla p &= \rho G \quad \text{in} \quad \Omega \\ \mathrm{div} \, u &= 0 \\ u &= u_+ \quad \text{on} \quad \Gamma_+ \\ u &= 0 \quad \text{on} \quad \Gamma_0 \\ pn - \mu \frac{\partial u}{\partial n} &= 0 \quad \text{on} \quad \Gamma_-,\end{aligned}$$

where Γ_+ is the inflow boundary, Γ_- is the outflow boundary, and Γ_0 is the fluid obstacle of which the shape is to be optimized. Here, $f : \mathbb{R}^3 \times \mathbb{R}^{3\times 3} \times \mathbb{R} \to \mathbb{R}$ and $g : \mathbb{R}^3 \times \mathbb{R}^3 \times \mathbb{R} \times \mathbb{R}^3 \to \mathbb{R}$ are assumed to be continuously differentiable in each argument. In order to keep the notation readable, components of the Jacobian are denoted as follows:

$$Du =: [a_{ij}]_{ij} \in \mathbb{R}^{3\times 3}$$

$$D_n u = Du \cdot n = \frac{\partial u}{\partial n} =: [b_i]_i \in \mathbb{R}^3.$$

The surface part g is chosen such that there exists a functional $\lambda : \Omega \to \mathbb{R}^d$ satisfying the following conditions on Γ_0:

$$\lambda_i = \frac{1}{\mu}\frac{\partial g}{\partial b_i} \; i = 1,2,3$$
$$\langle \lambda, n\rangle = -\frac{\partial g}{\partial p}.$$

A formal differentiation of the above leads to the gradient expression [8]

$$\begin{aligned} dJ(u,p,\Omega)[V] = &\int_{\Gamma_0} \langle V,n\rangle f(u,Du,p)dS + \int_{\Gamma_0}\langle V,n\rangle \\ &\times [D_{(u,b,p)}g(u,D_n u,p,n)\cdot n + \kappa g(u,D_n u,p,n)]dS \\ &+ \int_{\Gamma_0}\langle V,n\rangle\left[-\sum_{i=1}^{d}\left(\frac{\partial g}{\partial u_i} + \mu\frac{\partial \lambda_i}{\partial n} + \sum_{j=1}^{d}\frac{\partial f}{\partial a_{ij}}n_j\right)\frac{\partial u_i}{\partial n}\right]dS \\ &+ \int_{\Gamma_0}\langle V,n\rangle[(\mathrm{div}[\Gamma]\nabla_n g) - \kappa\langle \nabla_n g, n\rangle]dS, \end{aligned}$$

where $\nabla_n g$ denotes the vector consisting of components $\frac{\partial g}{\partial n_i}$ and λ and λ_p solve the adjoint incompressible Navier–Stokes equations

$$-\mu\Delta\lambda_i - \rho\sum_{j=1}^{d}\left(\frac{\partial \lambda_j}{\partial x_i}u_j + \frac{\partial \lambda_i}{\partial x_j}u_j\right) - \frac{\partial \lambda_p}{\partial x_i} = \frac{\partial f}{\partial u_i} - \sum_{j=1}^{d}\frac{\partial}{\partial x_j}\frac{\partial f}{\partial a_{ij}} \quad \text{in} \quad \Omega$$
$$\mathrm{div}\lambda = \frac{\partial f}{\partial p}$$

with boundary conditions

$$\lambda = 0 \quad \text{on} \quad \Gamma_+$$
$$\lambda_i = \frac{1}{\mu}\frac{\partial g}{\partial b_i} \quad \text{on} \quad \Gamma_0$$
$$\langle \lambda, n\rangle = -\frac{\partial g}{\partial p} \quad \text{on} \quad \Gamma_0$$
$$\mu\frac{\partial \lambda_i}{\partial n} + \rho\left(\sum_{j=1}^{d}\lambda_j u_j n_i + \lambda_i u_j n_j\right) + \lambda_p n_i = 0 \quad \text{on} \quad \Gamma_-.$$

2.4. Shape Hessian approximation and operator symbols

Very efficient optimization methods are usually variants of the SQP or Newton's method, which results in the need of higher order derivative information. However, shape Hessians are very complex objects and usually need to be approximated in some way. The above Navier–Stokes problem can be made into an excellent problem for studying shape Hessians. By choosing the constant density $\rho = 0$, the non-linearity vanishes. Coupled with the minimization of the kinetic energy dissipation, one arrives at the following problem where the fluid is modeled by the Stokes equations.

$$\min_{(u,p,\Omega)} J(u,p,\Omega) := \int_\Omega \mu\sum_{i,j=1}^{3}\left(\frac{\partial u_i}{\partial x_j}\right)^2 dA$$
$$\text{subject to} \; -\mu\Delta u + \nabla p = 0 \quad \text{in} \quad \Omega \; \mathrm{div}\, u = 0$$
$$u = u_+ \quad \text{on} \quad \Gamma_+ \; u = 0 \quad \text{on} \quad \Gamma_0$$
$$pn - \mu\frac{\partial u}{\partial n} = 0 \quad \text{on} \quad \Gamma_- \mathrm{Vol} = V_0.$$

The shape derivative of this problem is given by

$$dJ(u,p,\Omega)[V] = -\mu\int_{\Gamma_0}\langle V,n\rangle\sum_{k=1}^{3}\left(\frac{\partial u_k}{\partial n}\right)^2 dS, \tag{7}$$

which means the problem is self-adjoint and the Hessian can be studied without the need to consider variations in the adjoint multiplicators λ.

Shape gradients can be split in a geometric part, which stems from variations of the objective with respect to the geometry, (u,p) due to a change of the domain the PDE is defined on. The idea presented here from [9, 10] is to study the symbol of the control to state mapping of the dynamic part only. Considering a sinusoidal perturbation $\tilde{q}(x) = \hat{q}e^{i\omega x}$ of some control q, the pseudo-differential operator nature of the Hessian H can be seen by comparing the input $\tilde{q}$ with the output $H\tilde{q}$. For example, if

$$H\tilde{q} = i\omega\hat{q}e^{i\omega x} = i\omega\tilde{q}$$

then $\Sigma(\omega)$: = $i\omega$ is the symbol of the Hessian, and this corresponds to a classical differential operator of order +1. If, for example, one has

$$H\tilde{q} = -\omega^2\hat{q}e^{i\omega x} = -\omega^2\tilde{q}$$

then $\Sigma(\omega)$: = $-\omega^2$ is the symbol of the Hessian, and this corresponds to a classical differential operator of order +2. However, if

$$H\tilde{q} = |\omega|\hat{q}e^{i\omega x} = |\omega|\tilde{q},$$

then H is a pseudo-differential operator of order +1.

Assuming flow over a flat plate, the domain Ω is considered to be given by

$$\Omega = \{(x_1,x_2,x_3) \in \mathbb{R}^3 : x_3 \geqslant 0\}.$$

Thus, at the boundary $\Gamma = \{(x_1,x_2,x_3) \in \mathbb{R}^3 : x_3 = 0\}$, the outer normal is given by

$$n = (0,0,1)^T,$$

and a complex valued oscillation of the two dimensional flat plate is described by

$$x_3 = \alpha(x_1,x_2) := e^{i(\omega_1 x_1 + \omega_2 x_2)},$$

where i is the imaginary unit. Using this setting, the disturbed gradient from Eq. (7) is given by

$$\widetilde{G} := -2\mu\sum_{k=1}^{3}\frac{\partial u_k}{\partial n}\frac{\partial u_k'[\alpha]}{\partial n} = -2\mu\sum_{k=1}^{3}\frac{\partial u_k}{\partial x_3}\frac{\partial u_k'[\alpha]}{\partial x_3}$$

due to the flat initial domain under consideration. To identify the symbol of the Hessian, the mapping

$$S\alpha := -2\mu\sum_{k=1}^{3}\frac{\partial u_k}{\partial x_3}\frac{\partial u_k'[\alpha]}{\partial x_3}$$

must now be characterized by making α appear explicitly in the right hand side.

Furthermore, the perturbed states $u'[\alpha]$ and $p'[\alpha]$ are also considered to be oscillatory:

$$u_k'[\alpha] = \hat{u}_k e^{i(\omega_1 x_1 + \omega_2 x_2)}e^{\omega_3 x_3}$$
$$p'[\alpha] = \hat{p}e^{i(\omega_1 x_1 + \omega_2 x_2)}e^{\omega_3 x_3}.$$

The no-slip boundary condition on x_3 = 0 leads to

$$u_k'[\alpha] = \hat{u}_k\alpha e^0,$$

which results in

$$\hat{u}_k = -\frac{\partial u_k}{\partial x_3} \neq 0. \tag{8}$$

However, the linearized Stokes PDE must also be solved inside the domain. Applying the Laplace and gradient operator on the disturbances $u'[\alpha]$ and $p'[\alpha]$ is equivalent to

$$A\begin{pmatrix}\hat{u}_1\\ \hat{u}_2\\ \hat{u}_3\\ \hat{p}\end{pmatrix}\alpha(x_1,x_2)e^{\omega_3 x_3}=0,$$

where the matrix A can be thought of as the Stokes equation in the Fourier space. This is only non-contradictory to the consequences of the boundary condition (8), if the linearized system matrix A does not have full rank, which means the determinant of A must vanish:

$$\det(A)=\left[\mu(\omega_1^2+\omega_2^2-\omega_3^2)\right]^2(\omega_1^2+\omega_2^2-\omega_3^2)\overset{!}{=}0\Rightarrow\omega_3 =\pm\sqrt{\omega_1^2+\omega_2^2}.$$

Hence, it is possible to remove ω_3 from the equations and the local shape derivative of the velocity is given by

$$u_k'[\alpha]=-\frac{\partial u_k}{\partial x_3}\alpha e^{\pm\sqrt{\omega_1^2+\omega_2^2}x_3}\Rightarrow\frac{\partial u_k'[\alpha]}{\partial x_3}\Big|=\left[-\frac{\partial^2 u_k}{\partial x_3^2}\mp\frac{\partial u_k}{\partial x_3}\sqrt{\omega_1^2+\omega_2^2}\right]\alpha,$$

and the operator S is given by

$$S=-2\mu\sum_{k=1}^{3}\frac{\partial u_k}{\partial x_3}\left[-\frac{\partial^2 u_k}{\partial x_3^2}\pm\frac{\partial u_k}{\partial x_3}\sqrt{\omega_1^2+\omega_2^2}\right]. \tag{9}$$

In two dimensions, one can assume $\omega_2\equiv 0$ and the symbol becomes

$$\pm|\omega_1|,$$

which is the symbol of a pseudo-differential operator of order +1 closely related to the Dirichlet-to-Neumann map. For a true pseudo-differential operator with symbol $|\omega|$, a discretization using finite differences or surface finite elements is not straight forward. A symbol which can much more easily be approximated is ω^2, and this corresponds to the tangential Laplace operator, also known as Laplace–Beltrami operator Δ_Γ. Thus, the discrete Hessian is approximated by

$$H_h\approx k\Delta_\Gamma^h+I,$$

where $I\in\mathbb{R}^{m\times m}$ is the identity matrix for m surface mesh nodes and k is an appropriately chosen smoothing parameter.

2.5. Aerodynamic design using shape calculus

We conclude this section with the application of the above to a large scale aerodynamic design problem. The single set-point shape optimization of the "Very Efficient Large Aircraft (VELA)" blended wing-body aircraft is discussed. The inviscid fluid is modeled by the compressible Euler equations and the shape is to be optimized such that the pressure or wave drag in a transonic cruise of Mach 0.85 is minimized while the lift is kept constant. Thus, the optimization problem reads

$$\begin{aligned}&\min_{(\rho,u,E,\Omega)} C_D(\rho,u,E,\Omega)\\ &\text{subject to }\int_\Omega \operatorname{div}(\rho u)\,dA=0\\ &\qquad\int_\Omega\sum_{j=1}^{3}\left[\frac{\partial(\rho u_i u_j)}{\partial x_j}\right]+\frac{\partial p}{\partial x_i}dA=0\\ &\qquad\int_\Omega \operatorname{div}(\rho H u)\,dA=0\ \langle u,n\rangle=0\quad\text{on}\quad\Gamma_0\\ &\qquad C_L=C_{L_0}\ \text{Vol}=V_0.\end{aligned}$$

Here, the first three constraints are the Euler equations, and the pressure p is linked to the conserved variables

$$U:=(\rho,\rho u,\rho E)^T$$

by the perfect gas law

$$p=(\gamma-1)\rho\left(E-\frac{1}{2}\|u\|^2\right)$$

and H is the fluid enthalpy. The condition $\langle u,n\rangle = 0$ is the Euler slip boundary condition on the aircraft surface Γ. The farfield boundary conditions are usually more complex involving characteristics and are thought of as treated by the flow solver discretely.

Since the gradient based optimization method needs sensitivity information for both the objective function and the lift constraint, the generalized inviscid fluid forces

$$J(U,\Omega)=\int_{\Gamma_0}\langle p\cdot a,n\rangle dS \tag{10}$$

are considered, where a is a constant vector describing the rotation of the coordinate system, such that both drag, lift, and the appropriate angle of attack are considered simultaneously. The shape derivative of Eq. (10) is given by [11]

$$\begin{aligned}&dJ(U,\Omega)[V]\\ &=\int_{\Gamma_0}\langle V,n\rangle\left[\frac{\partial(p\cdot a)}{\partial n}n-\lambda U_H\left\langle\frac{\partial u}{\partial n},n\right\rangle\right.\\ &\qquad\left.+\operatorname{div}[\Gamma](p\cdot a-\lambda U_H u)\right]dS \qquad (11)\\ &=\int_{\Gamma_0}\langle V,n\rangle\left[\frac{\partial(p\cdot a)}{\partial n}n-\lambda U_H\left\langle\frac{\partial u}{\partial n},n\right\rangle+\kappa\langle p\cdot a,n\rangle\right]\\ &\qquad+\langle p\cdot a-\lambda U_H u,dn[V]\rangle\,dS. \qquad (12)\end{aligned}$$

Additionally, U_H is the vector of conserved variables with the last component replaced by ρH. The adjoint variables λ are given as the solution of [12,13]

$$\begin{aligned}&-A_1^T\frac{\partial}{\partial x_1}\lambda-A_2^T\frac{\partial}{\partial x_2}\lambda-A_3^T\frac{\partial}{\partial x_3}\lambda=0\quad\text{in}\quad\Omega\\ &\qquad\left\langle(\lambda_2,\lambda_3,\lambda_4)^T,n\right\rangle=-\langle a,n\rangle\quad\text{on}\quad\Gamma_0,\end{aligned}$$

where the A_i are the Euler flux Jacobians.

The VELA mesh consists of 115,673 surface nodes and 5,859,435 tetrahedra in the volume. Thus, there are approximately 29.3×10^6 unknowns for the fluid, which are computed using the DLR flow solver TAU. The planform of the aircraft is kept constant, such that 113,956 surface nodes of the CFD mesh are the design unknowns for the shape. At cruise condition of Mach 0.85 and 1.8° angle of attack, the initial drag value is $C_D = 4.77\times10^{-3}$ and the initial lift coefficient is $C_L = 1.787\times10^{-1}$. The initial and optimized shapes are shown in Fig. 1. The upper side transonic shock wave is completely removed, such that the optimized aircraft features a drag value of $C_D = 3.342\times10^{-3}$, an improvement by 30.06%, and the lift with $C_L = 1.775\times10^{-1}$ is kept within 0.67% of the original value. The optimization history is shown in Fig. 2.

3. Efficient treatment of uncertainties

In this section, we consider the shape optimization problem influenced by aleatory uncertainties which arises because of natural, unpredictable variations of the boundary conditions. Additional knowledge cannot reduce aleatory uncertainties, but it may be useful in getting a better characterization of the variability. In order to formulate the robust design optimization problem, the boundary conditions and input parameters are analyzed to identify

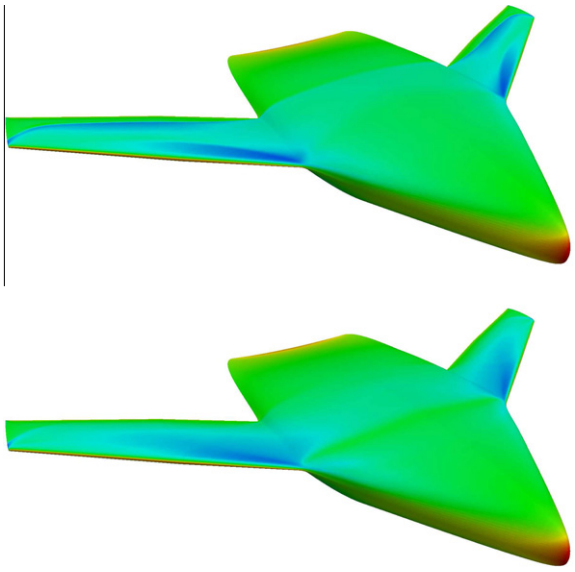

Fig. 1. Initial and optimized VELA aircraft. Color denotes pressure.

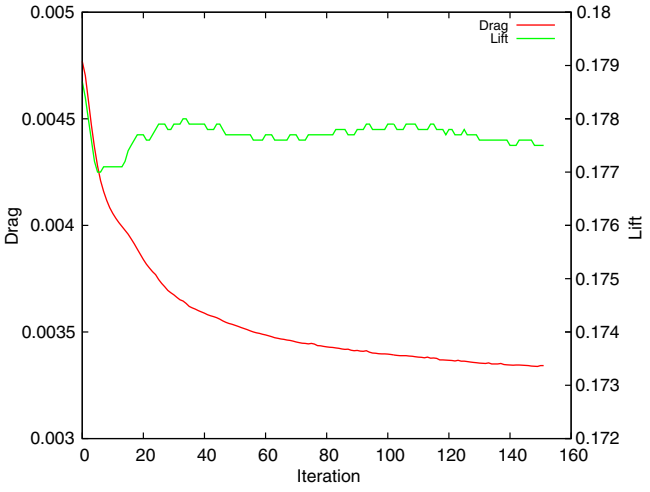

Fig. 2. Optimization history of the single set-point VELA aircraft. Note that the lift values are stored with three digits only.

the uncertainties which cannot be avoided at all before constructing an aircraft [14]. Beside the scalar-valued uncertainties , e.g. like angle of incidence, the velocity (Mach number) of the plane, in the macroscopic flight conditions, the aircraft geometry itself can be identified as an uncertainty source due to manufacturing tolerances, temporary factors like icing e.g. or fatigue of material. In the following, we will consider geometrical uncertainties in order to produce a design which is robust to small perturbations of the shape itself. In the literature, there can be found only a few papers on this topic investigating the influence of variations of the profile [15,16]. The general approach pursued in this paper is to apply a Karhunen–Loève-expansion to approximate the infinite-dimensional probability space modeling the geometrical uncertainties. The quantities of interest are expanded in a series of orthogonal polynomials by a non-intrusive Polynomial Chaos expansion to quantify the output of the solution with respect to the uncertainties. To overcome the curse of dimensionality an adaptively refined sparse grid is used.

3.1. Modeling geometrical uncertainties

The geometrical uncertainties depend on the geometry itself, so they are modeled as a Gaussian random field

$$\sigma : \Gamma \times \mathcal{O} \to \mathbb{R}, \tag{13}$$

defined on a probability space $(\mathcal{O}, \mathcal{A}, \mathcal{P})$ and on the shape of the airfoil Γ. In each point x of the shape Γ, the uncertainty is described by a normally distributed random variable $\sigma(x,\cdot) : \mathcal{O} \to \mathbb{R}$. Additionally, the second order statistics, the mean value and the covariance function, are given to fully describe the random field:

$$\mathbb{E}(\sigma(x,\omega)) = \sigma_0(x) = 0 \quad \forall x \in \Gamma,\ \omega \in \mathcal{O} \tag{14}$$

$$Cov(x,y) = b^2 \cdot \exp\left(-\frac{\|x-y\|^2}{l^2}\right) \quad \forall x,\ y \in \Gamma \tag{15}$$

The parameter l determines how quickly the covariance falls off and b controls the magnitude of the bumps. A squared exponential covariance function is chosen, since the resulting perturbed geometry is smooth due to the smoothness of the random field.

Then, a perturbed geometry is given as

$$v(x,\omega) = x + \sigma(x,\omega)\cdot\vec{n}(x) \qquad \forall x \in \Gamma, \omega \in \mathcal{O} \tag{16}$$

where $\vec{n}$ is the unit vector in x normal to the profile Γ. As we need to compute statistics of the aerodynamic flow depending on the uncertainty in our optimization algorithm, we have to approximate and discretize the probability space. This is performed by applying the Karhunen–Loève-expansion which provides an approximation of the random field σ for the numerical evaluation of such statistics.

3.2. Karhunen–Loève-expansion

The Karhunen–Loève (KL) expansion, also known as Proper Orthogonal Decomposition, represents the random field as a infinite linear combination of orthogonal functions chosen as the eigenfunctions of the covariance function [17,18]. The Karhunen–Loève-expansion of the Gaussian random field σ is given as:

$$\sigma(x,\omega) = \sigma_0(x) + \sum_{i=1}^{\infty}\sqrt{\lambda_i}z_i(x)Y_i(\omega) \tag{17}$$

$$= \sum_{i=1}^{\infty}\sqrt{\lambda_i}z_i(x)Y_i(\omega), \quad x \in \Gamma,\ \omega \in \mathcal{O} \tag{18}$$

where $\lambda_1 \geqslant \lambda_2 \geqslant \cdots \geqslant \lambda_i \geqslant \cdots \geqslant 0$ and z_i are the eigenvalues and eigenfunctions of the covariance function Cov which is symmetric and positive definite by definition. The deterministic eigenfunctions z_i are obtained from the spectral decomposition of the covariance function via solution of

$$\int_{\Gamma} Cov(x,y)z_i(y)dy = \lambda_i z_i(x), \quad x,y \in \Gamma. \tag{19}$$

Having the eigenpairs, the uncorrelated Gaussian random variables Y_i in Eq. (18) can be expressed as

$$Y_i(\omega) = \frac{1}{\sqrt{\lambda_i}}\int_{\Gamma}\sigma(x,\omega)z_i(x)dx, \quad \omega \in \mathcal{O},\ j = 1,2,\ldots \tag{20}$$

with zero mean and unit variance, i.e. $\mathbb{E}(Y_i) = 0$ and $\mathbb{E}(Y_iY_j) = \delta_{ij}$ for $j = 1,2,\ldots$ [19]. In the special case of a Gaussian random field, uncorrelated random variables are independent as well, which is an important property we will need later on for the sparse grid.

Truncating now the Karhunen–Loève-expansion after a finite number of terms, we obtain the approximation of the random field σ

$$\sigma_d(x,\omega) = \sum_{i=1}^{d}\sqrt{\lambda_i}z_i(x)Y_i(\omega), \qquad x \in \Gamma,\ \omega \in \mathcal{O}. \tag{21}$$

The corresponding covariance function is given by

$$Cov_d(x,y) = \sum_{i=1}^{d} \lambda_i z_i(x) z_i(y), \quad x,y \in \Gamma. \tag{22}$$

The eigenfunction basis $\{z_i\}$ is optimal in the sense that the mean square error resulting from the truncation after the dth term is minimized [20].

The following approximation error representation is then obtained by Mercer's theorem [21]

$$\lim_{d\to\infty} \left\{ \sup_{\Gamma} \int_{\mathcal{O}} (\sigma - \sigma_d)^2 \right\} = \lim_{d\to\infty} \left\{ \sup_{\Gamma} \left(\sum_{j=d+1}^{\infty} \lambda_j z_j^2 \right) \right\} = 0. \tag{23}$$

So, σ_d may provide a suitable approximation of σ, if the eigenvalues decay sufficiently fast and d is large enough [19]. If one assumes a Gaussian covariance function (cf. (15)), the eigenvalues will exponentially decay towards zero [22]. This paper [22] also provides a fast algorithm based on a kernel independent fast multipole method to compute the Karhunen–Loève approximation. Alternatively, a Krylov subspace method with a sparse matrix approximation using sparse hierarchical matrix techniques can be used to solve the large eigenvalue problem arising from the KL expansion [23].

3.3. Uncertainty quantification using Polynomial Chaos

In order to determine the effects of uncertainties in the input data on quantities of interest in the output of a simulation, we apply a non-intrusive Polynomial Chaos (PC) approach which was originally based on the theory of homogeneous chaos [24]. The basic idea of PC is the expansion of the stochastic outcome in a series of orthogonal polynomials with respect to the density function of the random input. We consider a function g depending on the state vector y, the design variables p and the approximated random field σ_d, e.g. the drag or the pressure distribution. Using a PC approach, g is expanded in a series of orthogonal polynomials with respect to the distribution of the random input vector σ_d

$$g(y,p,\sigma_d(\omega)) = g(y,p,Y_1(\omega),\dots,Y_d(\omega)) \tag{24}$$

$$= \sum_{i=1}^{\infty} g_i(y,p) \cdot \Phi_i(Y_1,\dots,Y_d) \tag{25}$$

with $g_i(y,p)$ deterministic coefficient functions, Φ_i multidimensional orthogonal polynomials determined by

$$\langle \Phi_n, \Phi_m \rangle = \int_{\mathcal{O}} \Phi_n(Y_1,\dots,Y_d)\Phi_m(Y_1,\dots,Y_d)\mathrm{d}\mathscr{P}(\omega)$$

$$= \begin{cases} = 0, & \text{if } n \neq m \\ \neq 0, & \text{if } n = m \end{cases}, \qquad \forall m,n \in \mathbb{N},$$

where $\mathscr{P}$ denotes the d-dimensional probability measure of the random vector $(Y_1,\dots,Y_d)$. Since the KL expansion of the Gaussian random field σ leads to a random vector σ_d of d independent Gaussian random variables, the stochastic outcome is expanded in a series of Hermite polynomials. As Eq. (25) indicates, the method allows a separation of the deterministic and stochastic part of the solution. In practice, one truncates the infinite expansion at a finite number of random variables and compute the statistics approximately by

$$g(y,p,\sigma_d(\omega)) \approx \sum_{i=1}^{M} g_i(y,p) \cdot \Phi_i(Y_1,\dots,Y_d). \tag{26}$$

Based on the theorem by Cameron and Martin [25], the unknown coefficients are given by

$$g_k(y,p) = \frac{\langle g(y,p,\cdot)\Phi_k \rangle}{\langle \Phi_k^2 \rangle} \tag{27}$$

$$= \frac{1}{\langle \Phi_k^2 \rangle} \int_{\mathcal{O}} g(y,p,Y_1,\dots,Y_d) \Phi_k(Y_1,\dots,Y_d)\mathrm{d}\gamma_d(\omega) \tag{28}$$

$k = 1,\dots,M$, where $\mathrm{d}\gamma_d(\omega)$ is the d-dimensional Gaussian measure. In the literature, there can be found a more in depth discussion of the non-intrusive PC approach [20,26,27].

3.4. Semi-infinite robust design

The usual single set-point aerodynamic shape optimization problem can be described in the following rather abstract form of an optimization problem with equality and inequality constraints

$$\min_{y,p} f(y,p) \tag{29}$$

$$\text{s.t.} c(y,p) = 0 \tag{30}$$

$$h(y,p) \geqslant 0 \tag{31}$$

Now, we think of Eq. (30) as the discretized outer flow equation around, e.g., an airfoil described by geometry parameter $p \in \mathbb{R}^{n_p}$. Rather than more general investigations on aerodynamic shape optimization [28], we assume that a finite parametrization of the shape to be optimized is given. The vector y is the state vector (velocities, pressure,...) of the flow model (30) and we assume that (30) can be solved uniquely for y for all reasonable geometries p. The objective in (29) $f : (y,p) \mapsto f(y,p) \in \mathbb{R}$ typically is the drag to be minimized. The restriction (31) typically denotes lift or pitching moment requirements. To make the discussion here simpler, we assume a scalar-valued restriction, i.e., $h(y,p) \in \mathbb{R}$. The generalization of the discussions below to more than one restriction is straight forward. In contrast to previous papers on robust aerodynamic optimization, we treat the angle of attack as a fixed parameter which is not adjusted to reach the required lift [29–31]. The general deterministic problem formulation (29)–(31) is influenced by stochastic perturbations. In the literature, min-max formulations and also chance constraint formulations can be found. According to our experience the semi-infinite formulation discussed below has been most successful. Here, the robust version of the nonlinear programming problem is written in the form of a semi-infinite optimization problem [30,32].

$$\min_{y,p} \mathbb{E}(f(y,p,\sigma(\cdot,\omega))) \tag{32}$$

$$\text{s.t.} c(y,p,\sigma(\cdot,\omega)) = 0, \quad \forall \omega \in \mathcal{O} \tag{33}$$

$$h(y,p,\sigma(\cdot,\omega)) \geqslant 0, \quad \forall \omega \in \mathcal{O} \tag{34}$$

Semi-infinite optimization problems have been treated directly so far only for rather small and weakly nonlinear problems [33]. In order to compute the mean in the objective function, we apply the KL expansion to the random field σ and replace f by the introduced PC approximation which leads to the following optimization problem

$$\min_{y,p} \mathbb{E}\left(\sum_{i=1}^{M} f_i(y,p) \cdot \Phi_i(Y_1,\dots,Y_d) \right) \tag{35}$$

$$\text{s.t.} c(y,p,\sigma_d(\cdot,\omega)) = 0, \quad \forall \omega \in \mathcal{O} \tag{36}$$

$$h(y,p,\sigma_d(\cdot,\omega)) \geqslant 0, \quad \forall \omega \in \mathcal{O}. \tag{37}$$

Due to the orthogonality of the Hermite polynomials Φ_k, (35)–(37) is equivalent to

$$\min_{y,p} \int_{\mathcal{O}} (f(y,p,Y_1,\ldots,Y_d)\mathrm{d}\gamma_d(\omega) \tag{38}$$

$$\text{s.t.} c(y,p,\sigma_d(\cdot,\omega)) = 0, \quad \forall \omega \in \mathcal{O} \tag{39}$$

$$h(y,p,\sigma_d(\cdot,\omega)) \geqslant 0, \quad \forall \omega \in \mathcal{O}. \tag{40}$$

For the numerical treatment of complicated design tasks, one has to approximate the integral in the objective (38) resulting in the form of a multiple set-point problem for the set-points $\{\sigma_d^i\}_{i=1}^N$:

$$\min_{y_i,p} \sum_{i=1}^{N} f(y_i,p,\sigma_d^i)v_i \tag{41}$$

$$\text{s.t.} c(y_i,p,\sigma_d^i) = 0, \quad \forall i \in \{1,\ldots,N\} \tag{42}$$

$$h(y_i,p,\sigma_d^i) \geqslant 0, \quad \forall i \in \{1,\ldots,N\}. \tag{43}$$

where v_i denote the quadrature weights. The discretized semi-infinite formulation (41)–(43) looks similar to the common deterministic multipoint approach. But one should be aware that the proposed stochastic formulations provide a more general framework for the treatment of uncertainties allowing the proper definition of measure of robustness and the integration of additional information of the uncertain input data. The weights v_i in (41) resulting from the numerical computation of the mean value (32) are based on the distribution of the input uncertainties. The approximation and discretization of the probability space using a goal-oriented KL expansion and an adaptive sparse grid strategy in order to formulate the introduced multiple set-point problem (41)–(43) are discussed in the following in more details.

3.5. Reduction of the dimension of the probability space using a goal-oriented Karhunen–Loève basis

Considering the integral (38), one term more in the truncated KL expansion to increase the approximation accuracy results in an integral of one dimension higher. In order to reduce the computational effort, the orthogonal basis functions $\{z_i\}$ will be chosen goal-oriented, i.e. the individual impact of the eigenvectors on the target functional will be taken into account. This method is well established in the model reduction methods of dynamic systems and the adaptive mesh refinement [34]. The idea is to develop an error indicator for the individual eigenvectors reflecting the influence on the drag. The introduced error analysis of the KL expansion only gives the approximation error of the random field σ, but not of the function of interest $f(y,p,\sigma)$. We propose to use sensitivity information to capture the local sensitivities of the drag with respect to the eigenvectors

$$\eta_i := \frac{\mathrm{d}f}{\mathrm{d}z_i} = -\lambda^\top \frac{\partial c}{\partial z_i} + \frac{\partial f}{\partial z_i}, \qquad \forall i = 1,\ldots,d \tag{44}$$

where λ solves the adjoint equation. The adjoint equation is independent of i, hence it has to be solved only once and the indicator η_i is numerically cheap to evaluate. Now, the reduced basis $\{\hat{z}_i\}$ can be automatically selected, the eigenvector z_i with a large value η_i have to be kept in the reduced basis, whereas a small value indicates that the basis vector can be rejected from the basis.

3.6. Locally refined dimension adaptive sparse grid for high-dimensional integration

Since the function evaluations are very expensive in our application, we introduce in this section an adaptive sparse grid strategy in order to further reduce the number of grid points but conserving the approximation quality. The reduction of computational effort can be achieved by using spatially adaptive or dimension-adaptive refinement [35,36]. The main advantage of the dimension-adaptive refinement strategy is the fact that one can use problem dependent quadrature formulas in order to construct the adaptive sparse grid. First, a generalization of sparse grids will be introduced which allows to weight the dimensions according to their importance on the target functional [36–39]. The original sparse grid S of order $\mathscr{J}$ combines all the incremental functions, defined as $\Delta^i = \mathscr{Q}^{i+1} - \mathscr{Q}^i$, $\mathscr{Q}^j$ 1D quadrature formula of order j, which sum up to order $\mathscr{J}$

$$S(\mathscr{J},d)(f) = \sum_{|\mathbf{i}| \leqslant \mathscr{J}} \left(\Delta^{i_1} \otimes \cdots \otimes \Delta^{i_d}\right)(f), \tag{45}$$

that means only those indices are considered which are contained in the unit simplex $|\mathbf{i}| \leqslant \mathscr{J}$. A more general index set is now allowed which can be adaptively chosen with respect to the importance of each dimension [36,40] . An index set I is called *admissible* if $\forall \mathbf{i} \in I$

$$\mathbf{i} - e_j \in I, \qquad \forall 1 \leqslant j \leqslant d,\ i_j > 1,$$

where $e_j \in \mathbb{R}^d$ is the jth unit vector. The generalized index set I contains for an index $\mathbf{i}$ all indices which have smaller entries in one or more dimensions. Due to this fact, the incremental sparse grid formula is still well defined for the new index sets and is given as

$$S(\mathscr{J},d)(f) = \sum_{\mathbf{i} \in I} \left(\Delta^{i_1} \otimes \cdots \otimes \Delta^{i_d}\right)(f). \tag{46}$$

The generalized definition of sparse grids includes the original sparse grid and the full tensor grid definition. Further, Eq. (46) particularly leaves more flexibility to the choice of the grids and therefore allows to handle anisotropic problems. In the following, an algorithm is introduced which automatically computes an admissible index set in a dimension adaptive way [36,40]. We start with the coarsest sparse grid, that means $I = \{(0,\ldots,0)\}$ and successively add new indices such that

- the new index set remains admissible
- the approximation error is reduced.

For the second point, an error indicator is needed. Taking a look at the difference formula (46), the term

$$\Delta_{\mathbf{i}} = \left(\Delta^{i_1} \otimes \cdots \otimes \Delta^{i_d}\right)(f) \tag{47}$$

indicates the reduction in the approximated integral for each new added index, so that we directly use $\Delta_{\mathbf{i}}$ as an error indicator for the adaptivity. As mentioned before, the main advantage of the dimension-adaptive refinement is the fact that the quadrature formulas can be chosen problem dependent. Considering geometry uncertainties described by a Gaussian random field, the Gauß–Hermite formulas are an appropriate choice for the quadrature. The Gauß–Hermite quadrature formulas are weakly nested, that means the rules of odd order all include the abscissa 0. Since the nesting is a favorable feature constructing the sparse grid, only the Gauß–Hermite quadrature of order 1, 3, 7, 15 are taken into account in the numerical results in order to construct the dimension adaptive sparse grid.

3.7. Numerically computed robust aerodynamic designs

The numerical solution strategy is based on the one-shot approach [41–44]. Additionally, we have employed an active set strategy, which uses the worst violation of the lift constraint as the active set in each iteration. The robust optimization under shape uncertainties of a transonic RAE2822 profile in Euler flow is considered. We use the flow solver TAU provided by DLR which allows the computation of gradients by the adjoint approach. The TAU Code is a CFD software package for the prediction of viscous and inviscid flows about complex geometries from the low subsonic to the hypersonic flow regime employing hybrid unstructured grids. The profile is described by 129 sur-

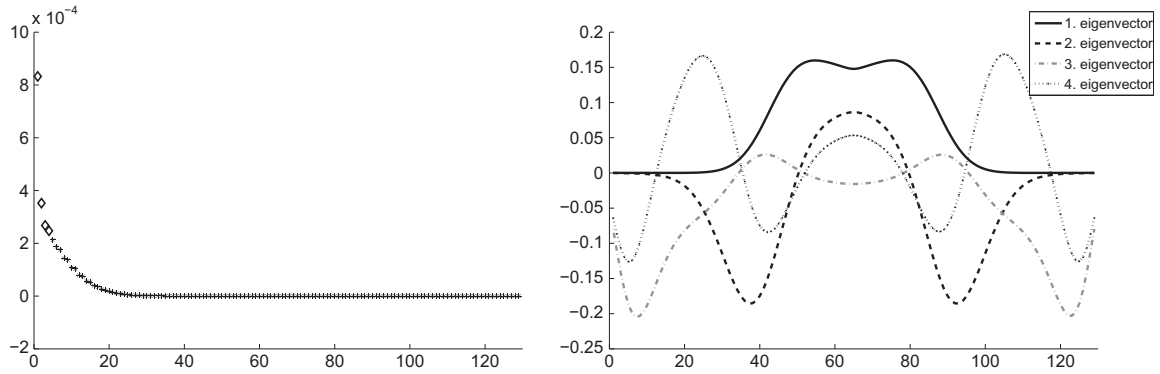

Fig. 3. Distribution of the eigenvalues and first four eigenvectors of the given random field σ.

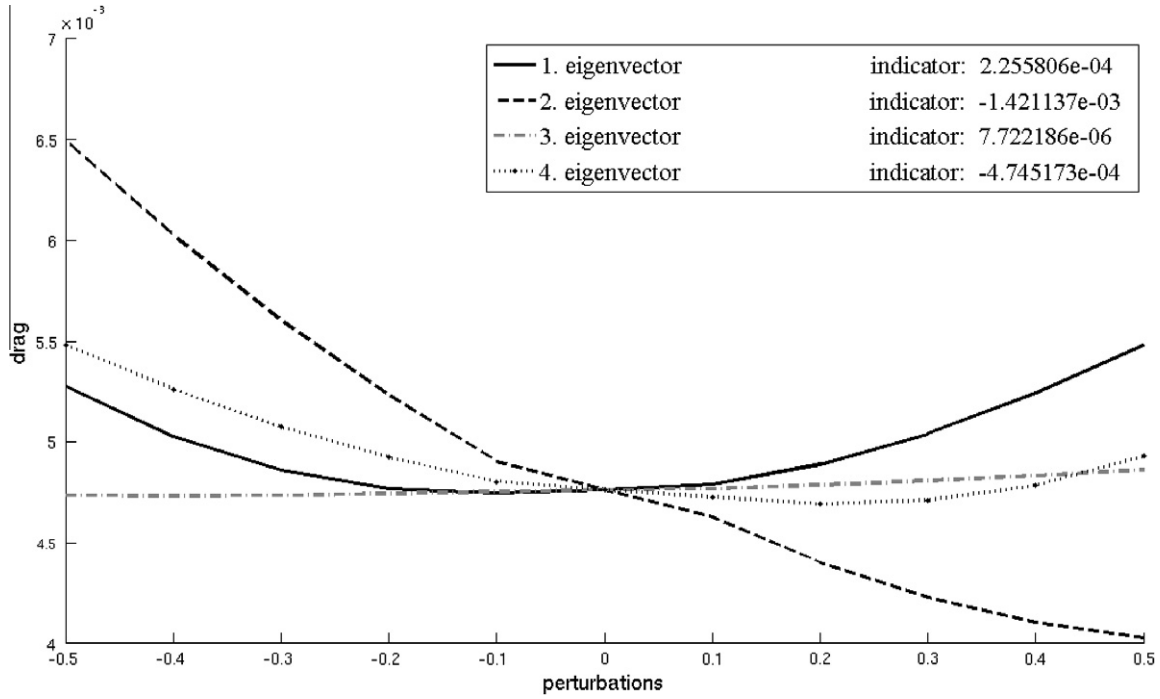

Fig. 4. Drag performance of the first four eigenvectors on the target functional.

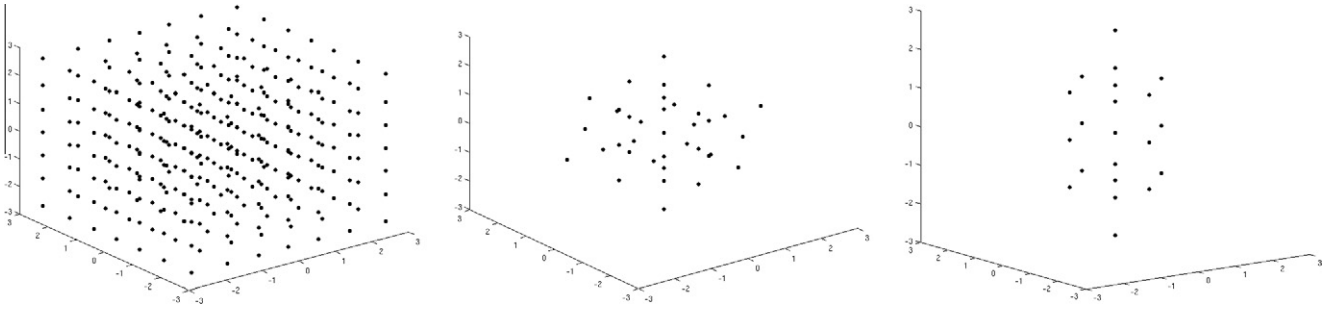

Fig. 5. Full tensor grid with 343 grid points, sparse grid with 37 grid points and dimension adaptive sparse grid with 21 grid points.

face grid points and the airfoil is parametrized by 21 Hicks–Henne functions. The geometry uncertainties are characterized by a Gaussian random field and the following second order statistics

$$\mathbb{E}(\sigma(x,\omega)) = 0 \qquad \forall x, y \in \Gamma \tag{48}$$

$$Cov(x,y) = (0.005)^2 \cdot \exp\left(-\frac{\|x-y\|^2}{(0.1)^2}\right) \tag{49}$$

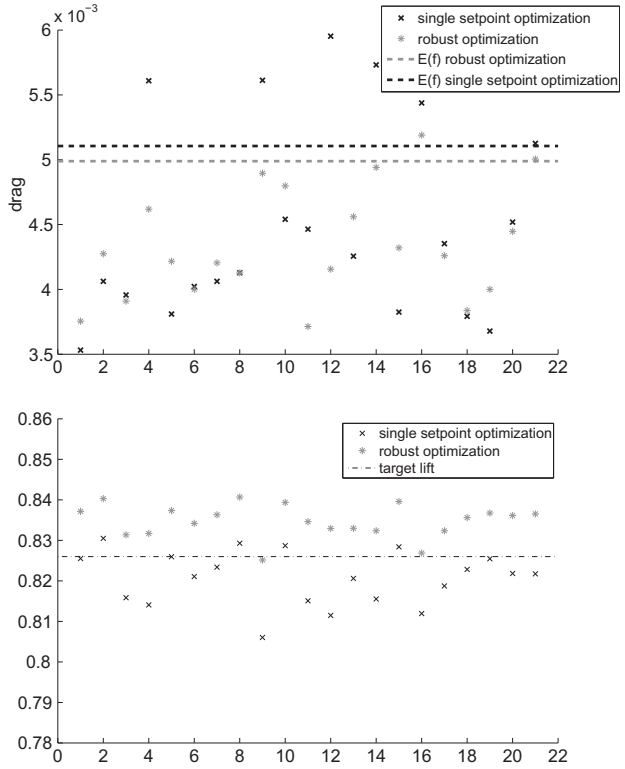

Fig. 6. Drag and lift performance of the 21 perturbed geometries.

The distribution of the eigenvalues using the KL expansion of the given random field (48) and (49) is shown in the next Fig. 3.

As stated before, the eigenvalues exponentially converge towards 0. For the numerical results below, we have considered only the first four eigenvalues and eigenvectors to represent the random field σ of perturbations. The corresponding eigenvectors are shown in Fig. 3. To further reduce the computational effort, we investigate the influence of the individual eigenvectors in order to reject those eigenvectors from the reduced basis which have no impact on the target functional. As Fig. 4 shows, the third eigenvector has no impact on the objective function, hence it can be rejected from the Karhunen–Loève basis and the dimension of the integral is reduced. This behaviour is also reflected by the introduced indicator.

The use of Gauß–Hermite formulas with an adaptive sparse grid strategy results in a grid consisting of 21 points for a given error tolerance of 10^{-5}. Compared to a full tensor grid approach, a reduction by factor 10 can be observed (cf. Fig. 5). The next Fig. 6 compare the results of the robust optimization and of the single set-point optimization, i.e. without considering any uncertainties in the optimization. The drag and lift performance is plotted against the 21 perturbed geometries and the dashed line in Fig. 6 indicates the mean value of the drag. The robust optimization improves the mean value of the target functional and also leads at the same time to a better lift performance over the whole range of perturbations, whereas the single set-point optimization is infeasible in more than the half of the considered grid points. Summing it all up, it can be said that the robust optimization leads to a better lift to drag ratio than the single set-point optimization and the resulting profile is more robust against small perturbations of the shape itself.

4. Conclusion

The discussions above demonstrate how the current state-of-the-art of deterministic parametric shape optimization for aircraft design can be improved significantly in terms of accuracy and efficiency by the usage of the shape calculus and in terms of practicability by employing robust design formulations for mitigating the effect of unavoidable uncertainties in the overall design problem formulation. It is to be expected that a combination of both methodologies leads to novel efficient, robust and accurate methods for aerodynamic design.

The extension of the methods presented here to the viscous laminar case, i.e. the compressible Navier–Stokes equations without turbulence modeling, is straight forward [10]. However, the popular Reynolds Averaged Navier–Stokes Equations (RANS) with turbulence modeling pose some difficulties for the shape calculus approach, as most turbulence models have elements that make the derivation of the analytic adjoint equations needed for shape calculus non-standard. However, this can easily be circumvented by considering a frozen eddy viscosity approach and there are also reports of successful uses of analytically adjointed turbulence models [45]. With respect to robust optimization and uncertainties, the inclusion of viscosity and substitute turbulence models is straight forward.

Acknowledgements

This research has been partly supported by the Deutsche Forschungsgemeinschaft within the Special Priority Programm "Optimization with Partial Differential Equations" (DFG SPP-1253) and by the German Federal Ministry of Economics and Labour (BMWA) within the collaborative effort MUNA under Contract No. 20A0604K. Furthermore, the authors thank Nicolas R. Gauger (RWTH Aachen), Caslav Ilic (DLR Braunschweig) and Alexander Litvinenko (TU Braunschweig) for fruitful collaboration and enlightning discussions on the subject.

References

[1] Schulz V, Gherman I. One-shot methods for aerodynamic shape optimization. In: Kroll N, Schwamborn D, Becker K, Rieger H, Thiele F, editors. MEGADESIGN and MegaOpt – German initiatives for aerodynamic simulation and optimization in aircraft design. Notes on numerical fluid mechanics and multidisciplinary design, vol. 107. Springer; 2009. p. 207–20.
[2] Haack W. Geschoßformen kleinsten Wellenwiderstandes. Bericht der Lilienthal-Gesellschaft 1941;136(1):14–28.
[3] Pironneau O. On optimum profiles in stokes flow. J Fluid Mech 1973;59(1):117–28.
[4] Hicks RM, Henne PA. Wing design by numerical optimization. J Aircraft 1978;15:407–12.
[5] Sokolowski J, Zolésio J-P. Introduction to shape optimization: shape sensitivity analysis. Springer; 1992.
[6] Delfour MC, Zolésio J-P. Shapes and geometries: analysis, differential calculus, and optimization. Adv Des Control. Philadelphia: SIAM; 2001.
[7] Rusinkiewicz S. Estimating curvatures and their derivatives on triangle meshes. In: Symposium on 3D data processing, visualization, and transmission; 2004.
[8] Schmidt S, Schulz V. Shape derivatives for general objective functions and the incompressible Navier–Stokes equations, Tech. Rep. Preprint SPP1253-10-05, DFG-SPP 1253. Control Cybern, in press.
[9] Schmidt S, Schulz V. Impulse response approximations of discrete shape Hessians with application in CFD. SIAM J Control Optimiz 2009; 48(4): 2562-80. URL <http://link.aip.org/link/?SJC/48/2562/1>.
[10] Schmidt S. Efficient large scale aerodynamic design based on shape calculus, Ph.D. thesis, University of Trier, Germany; 2010. URL <http://ubt.opus.hbz-nrw.de/volltexte/2010/569>.
[11] Schmidt S, Ilic C, Gauger N, Schulz V. Shape gradients and their smoothness for practical aerodynamic design optimization, Tech. Rep. Preprint-Nr.: SPP1253-10-03, DFG-SPP 1253, (submitted to OPTE); 2008.
[12] Giles MB, Pierce NA. Adjoint equations in CFD: duality, boundary conditions and solution behaviour, AIAA 97-1850.
[13] Gauger N. Das Adjungiertenverfahren in der aerodynamischen Formoptimierung, Ph.D. thesis, TU Braunschweig; 2003.
[14] Schulz V, Schillings C. On the nature and treatment of uncertainties in aerodynamic design. AIAA J. 2009;47(3):646–54.
[15] Gumbert C, Newman P, Hou G-W. High-fidelity computational optimization for 3-d flexible wings: part II – effect of random geometric uncertainty on design. Optimiz Eng 2005;6(1):139–56.

[16] Loeven G, Bijl H. Airfoil analysis with uncertain geometry using the probabilistic collocation method. In: 48th AIAA/ASME/ASCE/AHS/ASC structures, structural dynamics, and materials conference, AIAA 2008-2070; 2008.
[17] Karhunen K. Zur Spektraltheorie stochastischer Prozesse, Suomalaisen Tiedeakatemian toimituksia: Ser. A: 1. Math Phys 1946;34.
[18] Loeve M. Probability theory, vol. I and II. New York: Springer; 1978.
[19] Borzì A, von Winckel G. Multigrid methods and sparse-grid collocation techniques for parabolic optimal control problems with random coefficients. SIAM J Sci Comput 2009; 31(3): 2172-92. URL <http://link.aip.org/link/?SCE/31/2172/1>.
[20] Ghanem R, Spanos P. Stochastic finite elements: a spectral approach. New York: Springer-Verlag; 1991.
[21] Mercer J. Functions of positive and negative type and their connection with the theory of integral equations, Philos Trans Roy Soc Ldn. URL <http://en.wikipedia.org/wiki/Mercer's_theorem>.
[22] Schwab C, Todor R. Sparse finite elements for stochastic elliptic problems higher order moments. Computing 2003;71:43–63.
[23] Khoromskij BN, Litvinenko A, Matthies HG. Application of hierarchical matrices for computing the Karhunen–Loève expansion. Computing 2009;84(1-2): 49–67.
[24] Wiener N. The homogeneous chaos. Am J Math 1938; 60(4): 897–936. URL <http://www.jstor.org/stable/2371268>.
[25] Cameron RH, Martin WT. The orthogonal development of non-linear functionals in series of Fourier–Hermite functionals. Ann Math 1947; 48(2): 385–92. URL <http://www.jstor.org/stable/1969178>.
[26] Eldred M, Webster C, Constantine P. Evaluation of non-intrusive approaches for Wiener–Askey generalized polynomial chaos; 2008.
[27] Wan X, Karniadakis GE. Multi-element generalized polynomial chaos for arbitrary probability measures. SIAM J Sci Comput 2006;28(3):901–28.
[28] Eppler K, Schmidt S, Schulz V, Ilic C. Preconditioning the pressure tracking in fluid dynamics by shape Hessian information. J Optimiz Theory Appl 2009;141(3):513–31.
[29] Li W, Huyse L, Padula S. Robust airfoil optimization to achieve drag reduction over a range of mach numbers. Struct Multidiscip Optimiz 2002;24(1):38–50.
[30] Huyse L, Lewis R, Li W, Padula S. Probabilistic approach to free-form airfoil shape optimization under uncertainty. AIAA J 2002;40:1764–72.
[31] Padula S, Gumbert C, Li W. Aerospace applications of optimization under uncertainty. In: ISUMA '03: proceedings of the 4th international symposium on uncertainty modelling and analysis. Washington (DC, USA): IEEE Computer Society; 2003. p. 286.
[32] Li W, Padula SL. Robust airfoil optimization in high resolution design space, Tech. rep., ICASE NASA Langley Research Centre; 2003.
[33] Floudas C, Stein O. The adaptive convexification algorithm: a feasible point method for semi-infinite programming. SIAM J Optimiz 2007;18(4): 1187–208.
[34] Becker R, Braack M, Meidner D, Rannacher R, Vexler B. Adaptive finite element methods for pde-constrained optimal control problems. In: Reactive flows. Diffusion and transport. Springer; 2006. p. 177–205.
[35] Ma X, Zabaras N. An adaptive hierarchical sparse grid collocation algorithm for the solution of stochastic differential equations. J Comput Phys 2009;228(8): 3084–113.
[36] Gerstner T, Griebel M. Dimension-adaptive tensor-product quadrature. Computing 2003;71(1):65–87.
[37] Garcke J, Griebel M, Thess M. Data mining with sparse grids. Computing 2001;67(3):225–53.
[38] Bungartz H-J, Dirnstorfer S. Multivariate quadrature on adaptive sparse grids. Computing 2003;71(1):89–114.
[39] Klimke A. Uncertainty modeling using fuzzy arithmetic and sparse grids, Ph.D. thesis, Universität Stuttgart, Shaker Verlag, Aachen; 2006.
[40] Garcke J. A dimension adaptive sparse grid combination technique for machine learning. In: Read W, Larson JW, Roberts AJ, editors. Proceedings of the 13th biennial computational techniques and applications conference, CTAC-2006. ANZIAM J. 2007; 48: C725–40.
[41] Hazra S, Schulz V, Brezillon J, Gauger N. Aerodynamic shape optimization using simultaneous pseudo-timestepping. J Comput Phys 2005;204(1): 46–64.
[42] Hazra S, Schulz V. Simultaneous pseudo-timestepping for aerodynamic shape optimization problems with state constraints. SIAM J Sci Comput 2006;28(3): 1078–99.
[43] Schulz V, Gherman I. One-shot methods for aerodynamic shape optimization. In: Kroll N, Schwamborn D, Becker K, Rieger H, Thiele F, editors. MEGADESIGN and MegaOpt – German initiatives for aerodynamic simulation and optimization in aircraft design. Notes on numerical fluid mechanics and multidisciplinary design, Vol. 107. Springer; 2009. p. 207–20.
[44] Ito K, Kunisch K, Schulz V, Gherman I. Approximate nullspace iterations for KKT systems. SIAM J Matrix Anal Appl 2010;31(4):1835–47.
[45] Zymaris AS, Papadimitriou DI, Giannakoglou KC, Othmer C. Continuous adjoint approach to the Spalart–Allmaras turbulence model for incompressible flows. Comput Fluids 2009;38:1528–38.